Eulerian--Lagrangian Runge--Kutta Discontinuous Galerkin Method for Transport Simulations on Unstructured Meshes

Xiaofeng Cai[†]
and Jing-Mei Qiu[‡]

Abstract. The semi-Lagrangian (SL) approach is attractive in transport simulations, e.g., in climate modeling and kinetic models, due to its numerical stability in allowing extra-large time-stepping sizes. For practical problems with complex geometry, schemes on the unstructured meshes are preferred. However, accurate and mass conservative SL methods on unstructured meshes are still under development and encounter several challenges. For instance, when tracking characteristics backward in time, high order curves are required to accurately approximate the shape of upstream cells, which brings in extra computational complexity. To avoid such computational complexity, we propose an Eulerian--Lagrangian Runge--Kutta discontinuous Galerkin method (EL RK DG) in [X. Cai, J.-M. Qiu, and Y. Yang, *J. Comput. Phys.*, 439 (2021), 110392] as an extension of the SL discontinuous Galerkin (DG) methods. This work is a further extension of the algorithm to unstruc-tured triangular meshes with discussion on the treatment of the inflow boundary condition. We also discuss the discrete geometric conservation law. The nonlinear weighted essentially nonoscillatory (WENO) limiter is applied to control oscillations. Desired properties of the proposed method are numerically verified by a set of benchmark tests.

Key words. Eulerian--Lagrangian, discontinuous Galerkin, unstructured triangular meshes, mass conservation, semi-Lagrangian, characteristics

MSC codes. 65M25, 65M60, 76M10

DOI. 10.1137/21M1456753

1. Introduction.

Transport processes are ubiquitous in a variety of applications such as climate modeling and kinetic models. They can be described by the transport equation

$$u_t + \nabla \cdot (\mathbf{V}u) = 0, \tag{1.1}$$

where $\mathbf{V}$ is the advection coefficient, which could depend on space, time, and the solution u for a nonlinear problem.

In the past decades, extensive mesh-based computational tools such as Eulerian and semi-Lagrangian (SL) approaches have been successfully developed and applied to various areas of science and engineering. For the Eulerian approach, the Runge–Kutta (RK) discontinuous Galerkin (DG) methods [16] are well known for their properties of high resolution, compactness, flexibility for handling complex geometry, high parallel efficiency, and superconvergence for long time integration, which led to successful applications to diverse application fields such as aerodynamics [57], computational geosciences [50], and plasma simulation [14, 48] among many others. One drawback

Funding: This work was supported by NSF grant DMS-1818924, by Air Force Office of Scientific Research grant FA9550-18-1-0257, and by the University of Delaware.

[†] Advanced Institute of Natural Sciences, Beijing Normal University at Zhuhai, 519087, China, and Division of Science and Technology, United International College (BNU-HKBU), Zhuhai, 519087, China (xfcai@bnu.edu.cn, xiaofengcai@uic.edu.cn).

[‡] Department of Mathematical Sciences, University of Delaware, Newark, DE 19716, USA (jingqiu@udel.edu).

Accepted Manuscript
Version of record at: https://doi.org/10.1137/21M1456753

of the RK DG method is the stringent time-stepping size with numerical stability for explicit time stepping. On the other hand, the SL approach allows extra-large time-stepping size by tracking solutions along characteristics. Several classes of SL schemes have been developed such as the finite element based Lagrange–Galerkin method (or the characteristic Galerkin method) [39, 20, 36] and extensions [11, 44, 53, 46], finite difference based methods [40, 29], finite volume based methods [37, 24, 30, 34, 17], DG based methods [41, 43, 28, 31, 6, 5, 18], and unstructured meshes based methods [4, 3]. Recently, the multidimensional SLDG method was proposed in [8, 31]. For the nonlinear dynamics, the SL method can be coupled with the high order prediction-correction method [9] or the exponential integrators [7] for nonlinear characteristic tracing. For theoretical analysis, the optimal convergence and superconvergence of SLDG schemes for linear convection equations in one space dimension are shown in [54].

One significant limitation of the SL approach is efficient tracking of characteristics in a nonlinear, truly multidimensional, and highly accurate fashion. For example, in order to achieve third order spatial accuracy, sides of upstream cells have to be approximated by quadratic curves in a general setting. This introduces extra computational complexity, especially when extended to problems with dimension higher than two. In additional, to resolve the nonlinearity, some prediction-correction strategy or the exponential integrators [9, 7] have to be introduced. To address these challenges, we proposed a novel Eulerian–Lagrangian (EL) DG method in [10]. The EL DG method is a generalization of the SLDG method [8]. The SLDG method is formulated based on the design of a localized adjoint problem for the test function that exactly tracks characteristics, while in the EL DG method, the adjoint problem for the test function does not need to follow characteristics exactly; it only needs to follow them approximately. This feature allows flexibility, especially for high dimensional and nonlinear problems, where characteristics are difficult to track. The errors that occurred in approximating characteristics will be integrated in time by RK methods via the method-of-lines approach. Thus the fully discrete EL DG scheme will be termed the EL RK DG method. Note that the SLDG in [8] and the EL RK DG in [10] are based on the Cartesian meshes. With the consideration of complex geometry for practical applications, this paper extends the EL RK DG method to the unstructured triangular mesh.

We propose the EL schemes on the unstructured mesh that satisfy the following essential properties for transport problems: mass conservation, high order accuracy in both space and time, stability with extra-large time-stepping sizes, and essentially nonoscillatory for discontinuities. To conserve the total mass, the exact evaluation of the integral over the upstream cell that overlaps multiple background elements is crucial but very challenging. To tackle this difficulty, we propose a remapping algorithm by local mesh intersection that is mass conservative, where the evaluation of integrals is stable and accurate via a subregion-by-subregion fashion; other conservative remapping algorithms by local mesh intersection can be found in [2, 23, 22, 1]. We first propose a second order, unconditionally stable, and mass conservative SLDG method on the triangular meshes. Then we propose a high order EL RK DG method on the triangular meshes. Note that the evolution step of EL RK DG coincides with the arbitrary Lagrangian-Eulerian (ALE) DG scheme [26], from which we extend the discussion of discrete geometric conservation law (GCL) to the proposed EL RK DG method. In addition, we have discussions on the inflow boundary condition and nonlinear weighted essentially nonoscillatory (WENO) limiters [59] to control oscillations around discontinuities. As an initial effort, we confine our attention to the linear transport equations when $\mathbf{V}$ is independent of solution u.

The rest of this paper is arranged as follows. In section 2.2, we propose a second order conservative SLDG method on the unstructured mesh; in section 2.3, we propose a high order EL RK DG method on the triangular meshes together with the discussion on the discrete geometric conservation laws and the treatment of inflow boundary condition in sections 2.4 and 2.5, respectively. In section 3, we provide numerical results to showcase favorable properties of the proposed schemes. Finally, concluding remarks are made in section 4.

2. SLDG and EL RK DG on unstructured meshes.

2.1. A 2D transport problem and notation. We consider a 2D linear transport equation in a conservative form

$$u_t + \nabla_{x,y} \cdot (\mathbf{V}(x,y,t)u) = 0, \tag{2.1}$$

with continuous velocity field $\mathbf{V}(x,y,t) = (a(x,y,t), b(x,y,t))$ on a polygonal domain Ω, a given initial condition, and proper boundary conditions. In this paper, either the inflow/outflow or periodic boundary conditions will be considered. We generate a fixed background mesh which is a partition of Ω by a set of triangular elements K_j, $j = 1, \ldots, J$, and let $h = \sup_j \operatorname{diam}(K_j)$, where $\operatorname{diam}(K_j)$ denotes the diameter of K_j. We define the finite dimensional DG approximation space as $V_h^k = \{v_h : v_h|_{K_j} \in P^k(K_j)\}$, in which $P^k(K_j)$ denotes the space of polynomials in K_j of degree at most k. In particular, $P^k(K_j) = \operatorname{Span}(\Psi_i^{K_j} : i = 1, \ldots, n_k)$ with the dimension $n_k = \frac{(k+1)(k+2)}{2}$, where $\Psi_i^{K_j}, i = 1, \ldots, n_k$, are an orthogonal basis on K_j.

2.2. The SLDG method. In this section, we propose a conservative SLDG method on unstructured triangular meshes. The scheme uses linear functions to approximate sides of upstream cells. Note that the integral evaluations on the upstream cells that overlap with several background cells are important for mass conservation [36] and are performed by a new remapping algorithm, which is different from a direct application of numerical quadratures on the upstream cells [55]. It will be an important step for the higher order EL RK DG algorithm introduced next.

To update the numerical solution from time level t^n to time level t^{n+1} over element K_j, we consider an adjoint problem for the test function $\psi(x,y,t)$:

$$\psi_t + \mathbf{V}(x,y,t) \cdot \nabla_{x,y}\psi = 0, \; \psi(x,y,t=t^{n+1}) = \Psi(x,y) \in P^k(K_j), \tag{2.2}$$

for which the test function ψ stays constant along characteristic trajectories. As shown in [8], we have

$$\frac{d}{dt}\int_{K_j(t)} u(x,y,t)\psi(x,y,t)dxdy = 0,$$

where $K_j(t)$ is a dynamic moving element, emanating from the Eulerian element K_j at t^{n+1} backward in time by following the characteristic trajectories. The SLDG scheme is formulated as follows: given the approximate solution $u_h^n \in V_h^k$ at time level t^n, to find the solution $u_h^{n+1}|_{K_j} \in V_h^k$, such that for $\Psi_i^{K_j} \in P^k(K_j)$, $i = 1, \ldots, n_k$, we have

$$\int_{K_j} u_h^{n+1}\Psi_i^{K_j}(x,y)dxdy = \int_{K_j^\star} u_h^n \psi_i^{K_j}(x,y,t^n)dxdy, \tag{2.3}$$

Accepted Manuscript
Version of record at: https://doi.org/10.1137/21M1456753

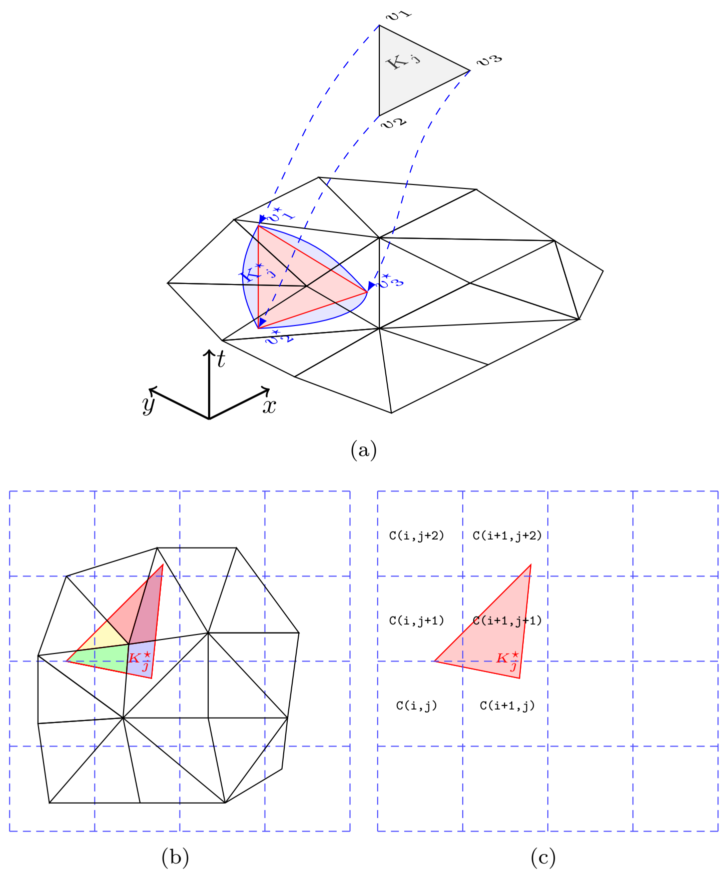

FIG. 1. *Illustration of SLDG with triangular approximation.* (c) $K_j^\star$ *connects the potential boxes:* `C(i,j)`, `C(i,j+1)`, `C(i,j+2)`, `C(i+1,j)`, `C(i+1,j+1)`, `C(i+1,j+2)`.

where $K_j^\star := K_j(t^n)$ denotes the upstream element of the element K_j following the characteristics backward to t^n (see the deformed element bounded by blue curves in Figure 1(a)), and $\psi_i^{K_j}(x, y, t^n)$ comes from tracking along characteristics from solving the final value adjoint problem (2.2).

The SLDG method boils down to evaluating the right-hand side (RHS) of (2.3), which consists of three parts: (1) the upstream element can be approximated by a triangle (subject to a second order accuracy), and below we still use $K_j^\star$ to represent this triangle, as shown in Figure 1; (2) $\psi_i^{K_j}(x, y, t^n)$ is unknown on $K_j^\star$, and we adopt an interpolation to reconstruct it based on the fact that the test function stays constant along characteristic trajectories; (3) u_h^n is the DG solution that is discontinuous across element interfaces of the background mesh (black lines in Figure 1(b)), and thus the evaluation of (2.3) should be evaluated in a subregion-by-region manner. Accordingly, the procedure of the SLDG method is performed as follows.

1. *Characteristic tracing.* The three vertices of K_j with the coordinate $(x_{j,q}, y_{j,q})$ are denoted by $v_q, q = 1, 2, 3$. We trace characteristic trajectories backward in time from time level t^{n+1} to time level t^n for v_q by using a high order RK

Accepted Manuscript
Version of record at: https://doi.org/10.1137/21M1456753

method to solve the characteristics equations,

$$\begin{cases} \frac{dx(t)}{dt} = a(x,y,t), \\ \frac{dy(t)}{dt} = b(x,y,t), \\ x(t^{n+1}) = x_{j,q}, y(t^{n+1}) = y_{j,q}, \end{cases}$$

and obtain $v_q^\star$ with the new coordinate $(x_{j,q}^\star, y_{j,q}^\star), q = 1,2,3$.

2. *Interpolation for test function* $\psi_i^{K_j}(x,y,t^n)$. We use a polynomial interpolation to approximate the test function $\psi_i^{K_j}(x,y,t^n)$, based on the fact that $\psi_i^{K_j}$ stays constant along characteristics; for instance, for $k=1$, we reconstruct a P^1 polynomial $\psi_i^{K_j^\star}(x,y)$ by the interpolation constraints $\psi_i^{K_j^\star}(x_{j,q}^\star, y_{j,q}^\star) = \Psi_i^{K_j}(x_{j,q}, y_{j,q}), q = 1,2,3$.
3. *An SLDG remapping algorithm.* When $K_j^\star$ overlaps with K_l in the background mesh, one can identify overlapping subregions (denoted by $K_{j,l}^\star$ and plotted in different colors in Figure 1(b)) and compute the integral (2.3) subregion-by-subregion. Subregions can be identified by an algorithm to determine the intersection regions illustrated in Figure 1(b), and the subregion integrals can be done by dividing subregions into triangles as in [32] (denoted by $K_{j,T_m}^\star$) and applying triangular quadrature rules in the reference element as in [31]. We denote the solution and test function at the quadrature point by $u_{i_g}^{K_{j,T_m}^\star}$ and $\psi_{i,i_g}^{K_{j,T_m}^\star}$, respectively. The corresponding weight and the area of $K_{j,T_m}^\star$ are denoted by w_{i_g}, $|K_{j,T_m}^\star|$. The formulation of this remapping algorithm is summarized as follows: for $K_j^\star$,

$$\begin{aligned} &\int_{K_j^\star} u_h(x,y,t^n)\psi_i^{K_j^\star}(x,y)dxdy \\ =&\sum_l \int_{K_{j,l}^\star} u_h(x,y,t^n)\psi_i^{K_j^\star}(x,y)dxdy \\ =&\sum_m \int_{K_{j,T_m}^\star} u_h(x,y,t^n)\psi_i^{K_j^\star}(x,y)dxdy \\ =&\sum_m \sum_{i_g} u_{i_g}^{K_{j,T_m}^\star} \psi_{i,i_g}^{K_{j,T_m}^\star} w_{i_g} |K_{j,T_m}^\star| := \tilde{U}_i^{K_j}(t^n). \end{aligned} \tag{2.4}$$

The key step of the remapping algorithm is to search $K_{j,l}^\star$, which is the overlapping subregion by the upstream element $K_j^\star$ and the Eulerian element K_l. Then we summarize the SLDG remapping algorithm as follows:

Step 1. To search the elements K_l that intersect with the upstream element $K_j^\star$, we generate an auxiliary rectangular mesh to create a location look-up table, with which we provide a look-up table for the location of K_l, as indicated in Figure 1(c).

Step 2. Perform the Sutherland–Hodgman clipping algorithm in [47, 13] for $K_j^\star$ and K_l to get $K_{j,l}^\star$ and cut it into a set of subtriangles $K_{j,T_m}^\star$.

Step 3. The final L^2 projection (2.4) can be done since given $K_{j,T_m}^\star$'s vertices and location in the background mesh, we can have $|K_{j,T_m}^\star|$, quadrature points, and corresponding $u_{i_g}^{K_{j,T_m}^\star}, \psi_{i,i_g}^{K_{j,T_m}^\star}$ in this subtriangle.

PROPOSITION 2.1. *Given a DG solution $u_h(x,y,t^n) \in V_h^k$ and assuming the boundary condition is periodic, the proposed SLDG scheme on the unstructured mesh*

Accepted Manuscript
Version of record at: https://doi.org/10.1137/21M1456753

(2.3) *is mass conservative. In particular,*

$$\sum_{j=1}^{J}\int_{K_j} u_h(x,y,t^{n+1})dxdy = \sum_{j=1}^{J}\int_{K_j} u_h(x,y,t^{n})dxdy. \tag{2.5}$$

Proof. The proof can be done by letting $\Psi(x,y) = 1$ and recombining $K^{\star}_{j,l}$ to the background mesh K_j as well as using the periodic boundary condition as that of SLDG on the structured mesh in [8]. ∎

2.3. The EL RK DG method. In this section, we propose a general high-order EL RK DG method on the unstructured triangular meshes, which is a generalization of the SLDG method [28, 8] and the RKDG method [16]. The proposed EL RK DG method is exactly mass conservative and largely alleviates the CFL condition of the RKDG method.

We start to formulate the EL RK DG scheme by a modified adjoint problem on the associated space-time region. The formulation can be viewed as a composition of the ALE scheme [26] and the SLDG remapping algorithm in the previous section.

(1) A modified adjoint problem for the 2D transport equation. Consider a *modified* adjoint problem:

$$\psi_t + \tilde{\mathbf{V}}(x,y,t)\cdot\nabla_{x,y}\psi = 0, \quad \psi(x,y,t=t^{n+1}) = \Psi(x,y) \in P^k(K_j), \tag{2.6}$$

where $\tilde{\mathbf{V}}(x,y,t) = (\alpha(x,y,t),\beta(x,y,t))$ are defined as follows:

1. *On* K_j *at* t^{n+1}. $\alpha(x,y,t^{n+1})$ and $\beta(x,y,t^{n+1})$ are set as P^1 polynomials denoted by

$$\alpha(x,y,t^{n+1}) = \alpha_0 + \alpha_1 x + \alpha_2 y, \tag{2.7}$$

$$\beta(x,y,t^{n+1}) = \beta_0 + \beta_1 x + \beta y. \tag{2.8}$$

As in [10], α and β are linear functions interpolating $\mathbf{V}(x,y,t)$ at vertices of K_j at the time level t^{n+1}.

2. *On* $\tilde{K}_j(t)$ *at* $t \in [t^n, t^{n+1})$. Along characteristic lines of the adjoint problem (2.6) originating from any point $(X,Y) \in K_j$ at t^{n+1}, with

$$\tilde{x}(t;(X,Y,t^{n+1})), \tilde{y}(t;(X,Y,t^{n+1})) \tag{2.9}$$

satisfying the following equations:

$$\frac{d}{dt}\tilde{x}(t;(X,Y,t^{n+1})) = \alpha(X,Y,t^{n+1}), \; \frac{d}{dt}\tilde{y}(t;(X,Y,t^{n+1})) = \beta(X,Y,t^{n+1}). \tag{2.10}$$

Note that the RHSs of the above equations are independent of t; then solving these equations that originate from (X,Y), we have

$$\tilde{x}(t;(X,Y,t^{n+1})) = X - \alpha(X,Y,t^{n+1})(t^{n+1}-t), \tag{2.11}$$

$$\tilde{y}(t;(X,Y,t^{n+1})) = Y - \beta(X,Y,t^{n+1})(t^{n+1}-t). \tag{2.12}$$

The associated space-time region for (2.6) then becomes $\tilde{\Omega}_j := \tilde{K}_j(t) \times [t^n, t^{n+1}]$, where $\tilde{K}_j(t)$ is the triangle with vertices along straight characteristic lines originated from vertices of K_j; see Figure 2(a).

Accepted Manuscript
Version of record at: https://doi.org/10.1137/21M1456753

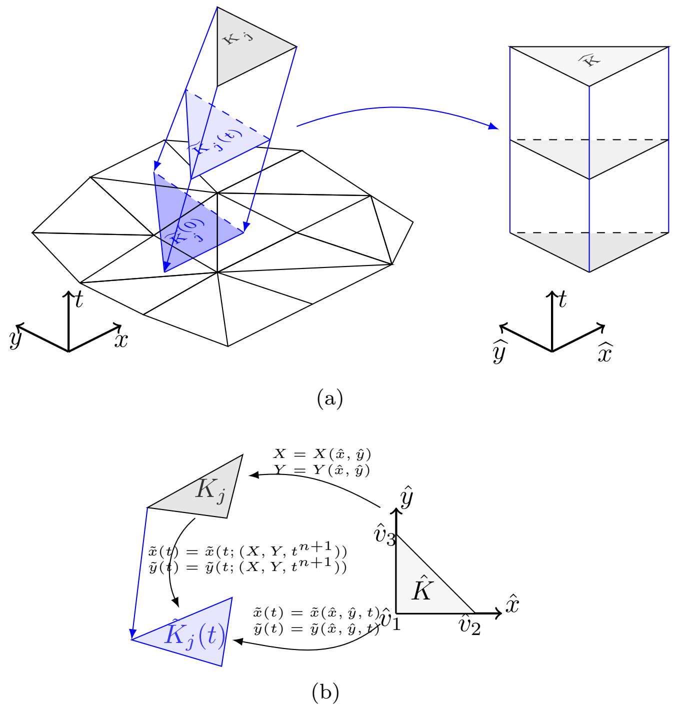

FIG. 2. (a) *Illustration of the space-time region* $\tilde{K}_j(t) \times [t^n, t^{n+1}]$. (b) *The mapping between dynamic element* $\tilde{K}_j(t)$ *and the reference element* $\hat{K}$.

Then, for $(\tilde{x}(t), \tilde{y}(t)) := \big(\tilde{x}(t; (X, Y, t^{n+1})), \tilde{y}(t; (X, Y, t^{n+1}))\big) \in \tilde{K}_j(t)$, where $t \in [t^n, t^{n+1}]$, the $\tilde{\mathbf{V}}(x, y, t)$ is defined as

$$\tilde{\mathbf{V}}(\tilde{x}(t), \tilde{y}(t), t) = \begin{pmatrix} \alpha\left(\tilde{x}(t; (X, Y, t^{n+1})), \tilde{y}(t; (X, Y, t^{n+1})), t\right) \\ \beta\left(\tilde{x}(t; (X, Y, t^{n+1})), \tilde{y}(t; (X, Y, t^{n+1})), t\right) \end{pmatrix} = \begin{pmatrix} \alpha(X, Y, t^{n+1}) \\ \beta(X, Y, t^{n+1}) \end{pmatrix}. \tag{2.13}$$

We summarize several properties of the modified adjoint problem in the following proposition.

PROPOSITION 2.2. *For the modified adjoint problem, we have the following:*
(i) *its characteristic lines,*

$$\tilde{x}(t; (X, Y, t^{n+1})), \tilde{y}(t; (X, Y, t^{n+1})), \tag{2.14}$$

for any point $(X, Y) \in K_j$ *at* t^{n+1}*, can be explicitly presented as*

$$\begin{pmatrix} \tilde{x}(t) \\ \tilde{y}(t) \end{pmatrix} = \mathbf{J}^{\tilde{K}_j K_j}(t) \begin{pmatrix} X \\ Y \end{pmatrix} + \begin{pmatrix} \delta_1(t) \\ \delta_2(t) \end{pmatrix}, \tag{2.15}$$

with the merely time-dependent Jacobian matrix denoted by

$$\mathbf{J}^{\tilde{K}_j K_j}(t) := \frac{\partial(\tilde{x}, \tilde{y})}{\partial(X, Y)}(t) := \begin{pmatrix} 1 - \frac{\partial \alpha}{\partial X}(t^{n+1} - t) & -\frac{\partial \alpha}{\partial Y}(t^{n+1} - t) \\ -\frac{\partial \beta}{\partial X}(t^{n+1} - t) & 1 - \frac{\partial \beta}{\partial Y}(t^{n+1} - t) \end{pmatrix}, \tag{2.16}$$

Accepted Manuscript
Version of record at: https://doi.org/10.1137/21M1456753

where $\delta_1(t) := (t - t^{n+1})\alpha_0, \delta_2(t) := (t - t^{n+1})\beta_0.$

(ii)

$$\psi(\tilde{x}(t;(x,y,t^{n+1})), \tilde{y}(t;(x,y,t^{n+1})), t) = \Psi(x,y) \in P^k(K_j) \ \forall t \in [t^n, t^{n+1}]. \tag{2.17}$$

Proof. First, the equation (2.15) can be easily obtained by substituting (2.7) and (2.8) into (2.11) and (2.12).

Second, we can prove (2.17) by the fact that the test function ψ stays constant along characteristics. ∎

(2) Semidiscrete EL RK DG formulation. Integrate $(2.1)\cdot\psi + (2.6)\cdot u$ over $\tilde{\Omega}_j$; that is,

$$\int_{\tilde{\Omega}_j} [(2.1)\cdot\psi + (2.6)\cdot u] dxdydt = 0. \tag{2.18}$$

After manipulating the above equation with the divergence theorem and the Leibniz–Reynolds transport theorem and considering its time differential form, we have

$$\frac{d}{dt}\int_{\tilde{K}_j(t)} u\psi dxdy = -\int_{\partial\tilde{K}_j(t)} \psi\mathbf{F}\cdot\mathbf{n}ds + \int_{\tilde{K}_j(t)} \mathbf{F}\cdot\nabla\psi dxdy, \tag{2.19}$$

where $\mathbf{F}(u,x,y,t) = (\mathbf{V}(x,y,t) - \tilde{\mathbf{V}}(x,y,t))u$, ds is the infinitesimal boundary of $\tilde{K}_j(t)$, and $\mathbf{n}$ denotes the unit outward normal vector to $\partial\tilde{K}_j(t)$.

To facilitate implementation, we map the semidiscrete EL RK DG formulation on the reference element $\hat{K}$ *with vertices* $\hat{v}_1(0,0)$, $\hat{v}_2(1,0)$, *and* $\hat{v}_3(0,1)$ *(see Figure* 2(b)*).* We denote the isoparametric mapping functions from the reference element $\hat{K}$ to the Eulerian element K_j and the dynamic element $\tilde{K}_j(t)$ by $(X(\hat{x},\hat{y}), Y(\hat{x},\hat{y}))^T$ and $(\tilde{x}(\hat{x},\hat{y},t), \tilde{y}(\hat{x},\hat{y},t))^T$, respectively. We can easily have

$$\begin{pmatrix} X(\hat{x},\hat{y}) \\ Y(\hat{x},\hat{y}) \end{pmatrix} = \mathbf{J}^{K_j\hat{K}_j} \begin{pmatrix} \hat{x} \\ \hat{y} \end{pmatrix} + \begin{pmatrix} x_{j,1} \\ y_{j,1} \end{pmatrix}, \tag{2.20}$$

where

$$\mathbf{J}^{K_j\hat{K}_j} = \begin{pmatrix} x_{j,2} - x_{j,1} & x_{j,3} - x_{j,1} \\ y_{j,2} - y_{j,1} & y_{j,3} - y_{j,1} \end{pmatrix}. \tag{2.21}$$

Then the mapping function $(\tilde{x}(\hat{x},\hat{y},t), \tilde{y}(\hat{x},\hat{y},t))^T$ can be presented as

$$\begin{aligned} \begin{pmatrix} \tilde{x}(\hat{x},\hat{y},t) \\ \tilde{y}(\hat{x},\hat{y},t) \end{pmatrix} &= \mathbf{J}^{\tilde{K}_jK_j}(t) \begin{pmatrix} X \\ Y \end{pmatrix} + \begin{pmatrix} \delta_1(t) \\ \delta_2(t) \end{pmatrix} \\ &= \mathbf{J}^{\tilde{K}_j\hat{K}_j}(t) \begin{pmatrix} \hat{x} \\ \hat{y} \end{pmatrix} + \mathbf{J}^{\tilde{K}_jK_j}(t) \begin{pmatrix} x_{j,1} \\ y_{j,1} \end{pmatrix} + \begin{pmatrix} \delta_1(t) \\ \delta_2(t) \end{pmatrix}, \end{aligned} \tag{2.22}$$

where $\mathbf{J}^{\tilde{K}_j\hat{K}_j}(t) = \mathbf{J}^{\tilde{K}_jK_j}(t)\mathbf{J}^{K_j\hat{K}_j}$, that is, the Jacobian of the mapping functions with respect to variables $\hat{x},\hat{y}$.

Next we introduce a few notations and useful equalities [15, 38] regarding this mapping function:

$$d\tilde{x}d\tilde{y} = \det\left(\mathbf{J}^{\tilde{K}_j\hat{K}_j}(t)\right) d\hat{x}d\hat{y}, \tag{2.23}$$

Accepted Manuscript
Version of record at: https://doi.org/10.1137/21M1456753

$$\nabla_{\tilde{x},\tilde{y}}\psi(\tilde{x},\tilde{y},t) = \mathbf{J}^{\tilde{K}_j\hat{K}_j}(t)^{-T}\nabla_{\hat{x},\hat{y}}\Psi(\hat{x},\hat{y}), \tag{2.24}$$

$$\mathbf{n}ds = \det\left(\mathbf{J}^{\tilde{K}_j\hat{K}_j}(t)\right)\mathbf{J}^{\tilde{K}_j\hat{K}_j}(t)^{-T}\check{\mathbf{n}}d\check{s}, \tag{2.25}$$

where $d\check{s}$ is the infinitesimal boundary of the isoparametric element and $\check{\mathbf{n}}$ denotes the unit outward normal vector to $\partial\hat{K}$.

We denote the approximation solution of u on the reference element by

$$\hat{u}_h(\hat{x},\hat{y},t) := \sum_{j=1}^{J}\sum_{p=1}^{n_k}\breve{u}_p^{K_j}(t)\hat{\Psi}_p^{K_j}(\hat{x},\hat{y}) := \sum_{p=1}^{Jn_k}\breve{u}_p(t)\hat{\Psi}_p(\hat{x},\hat{y}) \quad \forall t\in[t^n,t^{n+1}], \tag{2.26}$$

where $\hat{\Psi}_p^{K_j}(\hat{x},\hat{y})$ denotes $\Psi_p^{K_j}(X(\hat{x},\hat{y}),Y(\hat{x},\hat{y}))$, and we rename $\{\breve{u}_p^{K_j}(t) : 1\le p\le n_k, 1\le j\le J\} = \{\breve{u}_p(t) : 1\le p\le Jn_k\}$ and $\{\hat{\Psi}_p^{K_j} : 1\le p\le n_k, 1\le j\le J\} = \{\hat{\Psi}_p : 1\le p\le Jn_k\}$. We rewrite the semidiscrete EL RK DG formulation (2.19) on the reference element $\hat{K}$ as follows: $\forall\Psi_q(X,Y)\in V_h^k$,

$$\begin{aligned}&\frac{d}{dt}\int_{\hat{K}}\hat{u}_h\hat{\Psi}_q\det\left(\mathbf{J}^{\tilde{K}_j\hat{K}_j}(t)\right)d\hat{x}d\hat{y}\\ &= -\int_{\partial\hat{K}}\hat{\Psi}_q\widehat{F}d\check{s} + \int_{\hat{K}}\hat{\mathbf{F}}\cdot\left(\mathbf{J}^{\tilde{K}_j\hat{K}_j}(t)^{-T}\nabla_{\hat{x},\hat{y}}\hat{\Psi}_q\right)\det\left(\mathbf{J}^{\tilde{K}_j\hat{K}_j}(t)\right)d\hat{x}d\hat{y},\end{aligned} \tag{2.27}$$

where

$$\hat{\mathbf{F}}(\hat{u}_h,\hat{x},\hat{y},t) := \overline{\mathbf{V}}\hat{u}_h, \tag{2.28}$$

with

$$\overline{\mathbf{V}} := \left(\mathbf{V}(\tilde{x}(\hat{x},\hat{y},t),\tilde{y}(\hat{x},\hat{y},t),t) - \tilde{\mathbf{V}}(X(\hat{x},\hat{y}),Y(\hat{x},\hat{y}),t^{n+1})\right), \tag{2.29}$$

and we define the upwind numerical flux as

$$\widehat{F}\left(\hat{u}_h^{int_{\hat{K}}},\hat{u}_h^{ext_{\hat{K}}},\hat{x},\hat{y},t,\mathbf{J}^{\tilde{K}_j\hat{K}_j}(t)\right) = Wu^{\mathrm{up}} \tag{2.30}$$

with

$$W = \overline{\mathbf{V}}\cdot\left(\det\left(\mathbf{J}^{\tilde{K}_j\hat{K}_j}(t)\right)\mathbf{J}^{\tilde{K}_j\hat{K}_j}(t)^{-T}\check{\mathbf{n}}\right) \tag{2.31}$$

and

$$u^{\mathrm{up}} = \begin{cases}\hat{u}_h^{int_{\hat{K}}} & \text{if } W\ge 0,\\ \hat{u}_h^{ext_{\hat{K}}} & \text{if } W<0.\end{cases} \tag{2.32}$$

Here $\hat{u}_h^{int_{\hat{K}}}$ and $\hat{u}_h^{ext_{\hat{K}}}$ are the interior solution and the exterior solution of the $\tilde{K}_j(t)$, respectively. The line and volume integrals are performed by proper high order quadrature rules [21, 42] which are exact for polynomials of degree up to $2k$ for the element integral and up to $2k+1$ for the edge integral as in a standard RKDG scheme. Then we have

$$\frac{d}{dt}\int_{\hat{K}}\hat{u}_h\hat{\Psi}_q\det\left(\mathbf{J}^{\tilde{K}_j\hat{K}_j}(t)\right)d\hat{x}d\hat{y} = \mathcal{G}\left(\hat{u}_h,\mathbf{J}^{\tilde{K}_j\hat{K}_j}(t)\right), \tag{2.33}$$

Accepted Manuscript
Version of record at: https://doi.org/10.1137/21M1456753

where

$$\mathcal{G}\left(\hat{u}_h, \mathbf{J}^{\tilde{K}_j\hat{K}_j}(t)\right) := -\sum_{e\in\partial\hat{K}} |e| \sum_{i_e} \left[\hat{\Psi}_q \widehat{F}\right]\Big|_{(\hat{x}_{i_e},\hat{y}_{i_e})} \sigma_{i_e}$$

$$+2|\hat{K}|\sum_i \left[\hat{\mathbf{F}}\cdot\left(\mathbf{J}^{\tilde{K}_j\hat{K}_j}(t)^{-T}\nabla_{\hat{x},\hat{y}}\hat{\Psi}_q\right)\det\left(\mathbf{J}^{\tilde{K}_j\hat{K}_j}(t)\right)\right]\Big|_{(\hat{x}_i,\hat{y}_i)} w_i, \tag{2.34}$$

with the numerical quadrature points $(\hat{x}_{i_e}, \hat{y}_{i_e})$ and corresponding weights σ_{i_e} for the edge integral, and the numerical quadrature points $(\hat{x}_i, \hat{y}_i)$ and corresponding weights w_i for the element integral.

(3) Fully discrete EL RK DG scheme. We write the semidiscrete scheme (2.33) into a form of ordinary differential equations with the initial conditions. We let $\breve{\mathbf{u}}(t)$ be a vector in $\mathbb{R}^{Jn_k}$ which consists of unknowns $\{\breve{u}_p(t) : 1 \le p \le Jn_k\}$ and denote the spatial discretization operator of the RHS of (2.33) by $\mathcal{L}(\breve{\mathbf{u}}(t), t)$. Then the semidiscrete scheme (2.33) can be written as

$$\frac{d}{dt}\left(\mathbf{M}(t)\breve{\mathbf{u}}(t)\right) = \mathcal{L}\left(\breve{\mathbf{u}}(t), t\right), \quad \breve{\mathbf{u}}(t^n) = \breve{\mathbf{u}}^n, \tag{2.35}$$

where the matrix $\mathbf{M}(t) = \left(M_{pq}(t)\right)_{pq}$ with block diagonals,

$$\operatorname{diag}\left(\mathbf{M}^{K_1}(t), \ldots, \mathbf{M}^{K_J}(t)\right);$$

for $\mathbf{M}^{K_j}(t)$, its element

$$\begin{aligned}
M_{pq}^{K_j}(t) &= \int_{\hat{K}} \hat{\Psi}_p^{K_j}(\hat{x},\hat{y})\hat{\Psi}_q^{K_j}(\hat{x},\hat{y})\det\left(\mathbf{J}^{\tilde{K}_j\hat{K}_j}(t)\right)d\hat{x}d\hat{y}\\
&= \int_{\tilde{K}_j(t)} \psi_p^{K_j}(x,y,t)\psi_q^{K_j}(x,y,t)dxdy\\
&= \int_{K_j} \Psi_p^{K_j}(X,Y)\Psi_q^{K_j}(X,Y)\det\left(\mathbf{J}^{\tilde{K}_jK_j}(t)\right)dXdY\\
&= \det\left(\mathbf{J}^{\tilde{K}_jK_j}(t)\right)\int_{K_j} \Psi_p^{K_j}(X,Y)\Psi_q^{K_j}(X,Y)dXdY,
\end{aligned} \tag{2.36}$$

where the last equality is due to the space-independence of $\det(\mathbf{J}^{\tilde{K}_jK_j}(t))$. The following steps are proposed for updating the system (2.35).

1. *Building the space-time region.* In order to update the system (2.35) by the ALE scheme, we build the space-time region $\tilde{\Omega}$ and precompute the Jacobians at immediate stages of the RK method; the coordinates of vertices of the upstream element can be easily obtained from (2.11)–(2.12).
2. *The test function $\psi_p^{K_j}(x,y,t^n)$.* The test function $\psi_p^{K_j}(x,y,t^n)$ can be provided explicitly due to the local affine mapping (2.15).
3. *Remapping step.* We apply the remapping algorithm as proposed for the SLDG in section 2.2 to compute

$$\int_{K_j^\star} u_h^n \psi_p^{K_j}(x,y,t^n)dxdy := \tilde{U}_p^{K_j}(t^n). \tag{2.37}$$

We rename $\{\tilde{U}_p^{K_j}(t) : 1 \le p \le n_k, 1 \le j \le J\} := \{\tilde{U}_p(t) : 1 \le p \le Jn_k\}$, all elements of which form the vector $\tilde{\mathbf{U}}(t)$. Then the initial condition in (2.35) can be obtained as

$$\breve{\mathbf{u}}^n = \mathbf{M}(t^n)^{-1}\tilde{\mathbf{U}}(t^n), \quad p = 1\cdots Jn_k, \tag{2.38}$$

Accepted Manuscript
Version of record at: https://doi.org/10.1137/21M1456753

where $\mathbf{M}(t^n)$ comes from (2.36) and $\tilde{\mathbf{U}}(t^n)$ comes from (2.37) via the remapping algorithm.

4. *Evolution step.* We apply the strong stability preserving (SSP) RK method [45] to (2.35), which is organized in Algorithm 2.1. The parameters of the second order SSP-RK method (SSP-RK2) and the third order SSP-RK method (SSP-RK3) are provided in Table 1.

Algorithm 2.1 The s-stages SSP-RK time discretization for the system (2.35).

Let $\breve{\mathbf{u}}^{(0)} = \breve{\mathbf{u}}^n$; For RK stage $i = 1, \ldots, s$,

$$\breve{\mathbf{u}}^{(i)} = \mathbf{M}(t^n + d_i \Delta t^n)^{-1} \sum_{l=0}^{i-1} \left(\alpha_{il} \mathbf{M}(t + d_l \Delta t^n) \breve{\mathbf{u}}^{(l)} + \beta_{il} \Delta t^n \mathcal{L}\left(\breve{\mathbf{u}}^{(l)}, t^n + d_l \Delta t^n \right) \right), \tag{2.39}$$

where $\Delta t^n = t^{n+1} - t^n$, and α_{il} and β_{il} are related to the RK method;

$$\breve{\mathbf{u}}^{n+1} = \breve{\mathbf{u}}^{(s)}. \tag{2.40}$$

TABLE 1
Parameters of SSP-RK2 and SSP-RK3.

Order	α_{il}	β_{il}	d_l
2	1	1	0
	$\frac{1}{2}$ $\frac{1}{2}$	0 $\frac{1}{2}$	1
3	1	1	0
	$\frac{3}{4}$ $\frac{1}{4}$	0 $\frac{1}{4}$	1
	$\frac{1}{3}$ 0 $\frac{2}{3}$	0 0 $\frac{2}{3}$	$\frac{1}{2}$

PROPOSITION 2.3. *Given a DG solution $u_h(x, y, t^n) \in V_h^k$ and assuming the boundary condition is periodic, the fully discrete EL RK DG scheme with SSP-RK time discretization on the unstructured mesh is mass conservative.*

Proof. The conclusion is due to the mass conservative of the SLDG remapping algorithm and the local conservative form of the integrating flux function with the unique flux at the element boundaries. We skip the details for brevity. ∎

Remark 2.4. (comparison to the ALE DG method [26]) We note that when we put the background element K_j at t^{n+1} and its upstream element $K_j^\star$ at t^n in a moving mesh setting, the formulation of EL RK DG scheme (2.19) is the same as the ALE DG method [26] and the quasi-Lagrangian moving mesh DG method [35]. In fact, the EL RK DG method for the problem (2.35) is the composition of the SLDG remapping algorithm in evaluating $\breve{\mathbf{u}}(t^n)$ and the ALE DG method in updating solutions from $\breve{\mathbf{u}}(t^n)$ to $\breve{\mathbf{u}}(t^{n+1})$.

Remark 2.5. (empirical time step constraint for stability) Note that the time step constraints for the RKDG scheme on triangular meshes are numerically verified in [16, 12] as around

$$\Delta t \sim \frac{\min_j R_j}{\max_j \max_{\text{face}} |\mathbf{V} \cdot \mathbf{n}|}. \tag{2.41}$$

We observe that the EL RK DG formulation is similar in spirit to applying the RKDG method with the flux term $(\mathbf{V} - \tilde{\mathbf{V}})u$; thus an empirical time step stability constraint

Accepted Manuscript
Version of record at: https://doi.org/10.1137/21M1456753

of the EL RK DG method is

$$\Delta t \sim \frac{\min_j R_j}{\max_j \max_{\text{face}} |(\mathbf{V}-\tilde{\mathbf{V}})\cdot \mathbf{n}|}. \tag{2.42}$$

For a smooth velocity field $\mathbf{V}$, by Taylor expansions, we have $|(\mathbf{V}-\tilde{\mathbf{V}})\cdot\mathbf{n}| = O(\Delta t)+O(h^2)$. Combining the estimate with (2.42) gives the time step constraint for the stability of the EL RK DG scheme on the unstructured triangular mesh,

$$\Delta t \sim \sqrt{h}. \tag{2.43}$$

This is verified in Example 3.3 with mesh refinement; that is, we refine the mesh by increasing the number of elements by a factor of around 4, and then the maximum CFL with numerical stability could increase by a factor of around $\sqrt{2}$. A rigorous analysis is subject to further investigation.

2.4. Geometric conservation law. Although the EL RK DG scheme is a fixed mesh method, we notice that an ALE scheme is embedded in the EL RK DG scheme (2.35). Hence, the GCL introduced in [51, 49, 25], i.e., the preservation of constant solutions, should be considered; that is, by letting $\hat{u}_h$ and $\hat{\Psi}_q$ be a constant, the obtained formulation in the following should be updated by numerical schemes exactly.

PROPOSITION 2.6. *Letting $\hat{u}_h = \hat{\Psi}_q = c$ and assuming the divergence-free property of $\mathbf{V}$ (i.e., $\nabla_{\hat{x},\hat{y}}\cdot\mathbf{V}=0$), the semidiscrete EL RK DG formulation on the reference element $\hat{K}$ (2.27) can be written as follows:*

$$\frac{d}{dt}\det\left(\mathbf{J}^{\tilde{K}_j\hat{K}_j}(t)\right) = \left(\nabla_{\hat{x},\hat{y}}\cdot\left(\mathbf{J}^{\tilde{K}\hat{K}}(t)^{-1}\tilde{\mathbf{V}}(X(\hat{x},\hat{y}),Y(\hat{x},\hat{y}),t^{n+1})\right)\right)\det\left(\mathbf{J}^{\tilde{K}_j\hat{K}_j}(t)\right). \tag{2.44}$$

Proof. It can be proven by substituting $\hat{u}_h = \hat{\Psi}_q = c$ into (2.27) and then using $\nabla_{\hat{x},\hat{y}}\cdot\mathbf{V}=0$, the linear property of $\tilde{\mathbf{V}}$, and integration by parts. ∎

Note that the scheme (2.35) by the SSP-RK method fails to preserve the constant solution since the Jacobian determinant $\det(\mathbf{J}^{\tilde{K}_j\hat{K}_j}(t))$ is involved in both sides of (2.44) and is evolved approximately due to the temporal integration.

To preserve the constant solution, we need to consider the time discretization of the evolution of the Jacobian determinant (2.44) as well; we adopt the GCL correction strategy by updating the Jacobian determinant by the SSP-RK method synchronously, which was introduced in [38, 26, 56]. For implementation, we replace the system (2.35) by

$$\frac{d}{dt}\left(\widetilde{\mathbf{M}}(t)\check{\mathbf{u}}(t)\right) = \mathcal{L}\left(\check{\mathbf{u}}(t),t\right), \quad \check{\mathbf{u}}(t^n)=\check{\mathbf{u}}^n, \tag{2.45}$$

$$\frac{d}{dt}\mathcal{J}_j(t) = \left(\nabla_{\hat{x},\hat{y}}\cdot\left(\mathbf{J}^{\tilde{K}\hat{K}}(t)^{-1}\tilde{\mathbf{V}}(X(\hat{x},\hat{y}),Y(\hat{x},\hat{y}),t^{n+1})\right)\right)\det\left(\mathbf{J}^{\tilde{K}_j\hat{K}_j}(t)\right) := \mathcal{R}(t), \tag{2.46}$$

where $\mathcal{J}_j(t)$ is an approximation to $\det(\mathbf{J}^{\tilde{K}_j\hat{K}_j}(t))$, $\mathcal{J}_j(t^n)=\det(\mathbf{J}^{\tilde{K}\hat{K}}(t^n))$, and the matrix $\widetilde{\mathbf{M}}(t) = (\widetilde{M}_{pq}(t))_{pq}$ with block diagonals $\operatorname{diag}(\widetilde{\mathbf{M}}^{K_1}(t),\ldots,\widetilde{\mathbf{M}}^{K_J}(t))$. The element of $\widetilde{\mathbf{M}}^{K_j}(t)$ is set as

$$\widetilde{M}^{K_j}_{pq}(t) = M^{K_j}_{pq}(t)\frac{\mathcal{J}_j(t)}{\det\left(\mathbf{J}^{\tilde{K}_j\hat{K}_j}(t)\right)}. \tag{2.47}$$

Accepted Manuscript
Version of record at: https://doi.org/10.1137/21M1456753

Algorithm 2.2 The s-stages SSP-RK time discretization for the system (2.45)–(2.46).

Let $\mathcal{J}_j^{(0)} = \mathcal{J}_j(t^n)$;

$$\int_{\hat{K}} \hat{u}_h^{(0)} \hat{\Psi}_q \mathcal{J}_j^{(0)} d\hat{x}d\hat{y} = \int_{\hat{K}} \hat{u}_h^n \hat{\Psi}_q \mathcal{J}_j(t^n) d\hat{x}d\hat{y}; \tag{2.48}$$

For RK stage $i = 1, \ldots, s$,

$$\mathcal{J}_j^{(i)} = \sum_{l=0}^{i-1} \left(\alpha_{il} \mathcal{J}_j^{(l)} + \beta_{il} \Delta t^n \mathcal{R}\left(t^n + d_l \Delta t^n\right) \right); \tag{2.49}$$

$$\begin{aligned} &\int_{\hat{K}} \hat{u}_h^{(i)} \hat{\Psi}_q \mathcal{J}_j^{(i)} d\hat{x}d\hat{y} \\ &= \sum_{l=0}^{i-1} \left(\alpha_{il} \int_{\hat{K}} \hat{u}_h^{(l)} \hat{\Psi}_q \mathcal{J}_j^{(l)} d\hat{x}d\hat{y} + \beta_{il} \Delta t^n \mathcal{G}\left(\hat{u}_h^{(l)}, \mathbf{J}^{\tilde{K}_j \hat{K}_j}(t^n + d_l \Delta t^n) \right) \right); \end{aligned} \tag{2.50}$$

$$\int_{\hat{K}} \hat{u}_h^{n+1} \hat{\Psi}_q \det\left(\mathbf{J}^{\tilde{K}_j \hat{K}_j}(t^{n+1}) \right) d\hat{x}d\hat{y} = \int_{\hat{K}} \hat{u}_h^{(s)} \hat{\Psi}_q \mathcal{J}_j^{(s)} d\hat{x}d\hat{y}. \tag{2.51}$$

Then we apply the s-stages SSP-RK method to the system to replace the evolution step in the EL RK DG method, which is organized in Algorithm 2.2.

Finally, we state that the EL RK DG scheme with (2.37)–(2.38) and the evolution step of Algorithm 2.2 satisfies the GCL when the RHS of (2.27) (for instance, the problem with the velocity field being merely time-dependent, i.e., $\mathbf{V}(t) = (\bar{a}(t), \bar{b}(t))$) can be solved exactly by the numerical quadratures, which is summarized in the following proposition.

PROPOSITION 2.7 (discrete geometric conservation law). *Suppose that the RHS of* (2.27) *can be solved exactly by the numerical quadratures, an s-stage SSP-RK method with order greater than or equal to* 2, *and the solution at time level t^n, $u_h^n = c$ for all $(x, y) \in \Omega$. Then the solution at time level t^{n+1} of the EL RK DG scheme with* (2.37)–(2.38) *and the evolution step of Algorithm* 2.2 *is $u_h^{n+1} = c$ for all $(x, y) \in \Omega$.*

Proof. As in Remark 2.4, the EL RK DG method for the problem (2.35) is the composition of the SLDG remapping algorithm in evaluating $\breve{\mathbf{u}}(t^n)$ and the ALE DG method. For the SLDG remapping algorithm, it is easy to see that when $u_h^n = c$ for all $(x, y) \in \Omega$, through the remapping algorithm (2.37) and mapping solution to the reference element (2.38), we have $\hat{u} = c$. Then similar to the proof of the GCL property of ALE DG in [26], we can show that $u_h^{n+1} = c$ and thus omit the details. ∎

2.5. Inflow boundaries. In this section, we consider the inflow Dirichlet boundary conditions, which are often posed in applications such as subsurface contaminant transport and remediation [52]. For inflow boundary conditions, we propose a ghost-cell strategy.

Let $\partial\Omega$ be the boundary of Ω, and let $\Gamma := \partial\Omega \times (0, T)$, consisting of two parts: the inflow part Γ_{in} and outflow part Γ_{out} with

$$\Gamma_{\text{in}} := \{(x, y, t) | (x, y) \in \partial\Omega, t \in (0, T), \mathbf{V} \cdot \mathbf{n} < 0\}, \ \Gamma_{\text{out}} = \Gamma \setminus \Gamma_{\text{in}}.$$

Accepted Manuscript
Version of record at: https://doi.org/10.1137/21M1456753

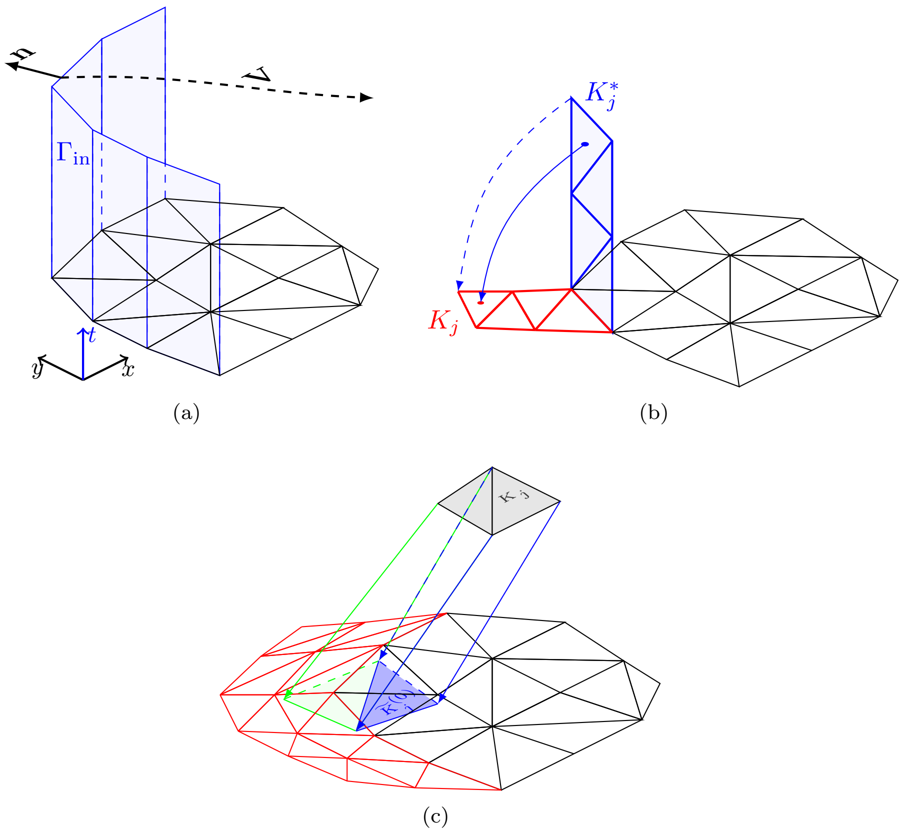

Fig. 3. *The illustration of the EL RK DG scheme on the ghost-cells method for transport problems with inflow boundary conditions.*

We consider the transport problem (2.1) with the inflow Dirichlet boundary condition

$$u(x,y,t) = g(x,y,t),\ (x,y,t) \in \Gamma_{\text{in}}.$$

The scheme proceeds on a large enough ghost region by first building DG solutions on ghost cells by a Lagrangian procedure. Once this is done, the EL RK DG scheme in section 2.3 can be implemented, as illustrated in Figure 3(c). The procedure of building DG solutions on ghost cells consists of several steps:

1. Generate a set of triangular elements K_j^* on the Γ_{in}.
2. Locate the vertices of the ghost element K_j by tracking the characteristics

$$\begin{cases} \frac{dx(t)}{dt} = a(x,y,t), \\ \frac{dy(t)}{dt} = b(x,y,t), \\ x(t^*) = x^*_{j,q},\ y(t^*) = y^*_{j,q}, \end{cases} \tag{2.52}$$

where $(x^*_{j,q}, y^*_{j,q}, t^*)$ are the coordinates of the vertex of element K_j^*, as illustrated in Figure 3(b). We denote the region which originates from K_j^* to K_j along the characteristics by $\mathcal{K}$. Note that the velocity field $\mathbf{V}(x,y,t)$ outside of Ω is the natural extension of the velocity field in Ω.

3. We consider the adjoint problem for the test function ψ,

$$\psi_t + \mathbf{V}(x, y, t) \cdot \nabla_{x,y}\psi = 0,\ \psi(x, y, t = t^n) = \Psi(x, y) \in P^k(K_j). \tag{2.53}$$

Integrate (2.1) $\cdot\, \psi$ + (2.53) $\cdot\, u$ over $\mathcal{K}$, that is,

$$\int_{\mathcal{K}} [(2.1) \cdot \psi + (2.6) \cdot u] dxdydt = 0. \tag{2.54}$$

After manipulating the above equation with the divergence theorem, we have

$$\int_{K_j} u\Psi dxdy = \int_{K_j^*} (\mathbf{V}(x, y, t)u\psi) \cdot \mathbf{n} dS, \tag{2.55}$$

where dS is infinitesimal of K_j^*. We adopt the SLDG scheme in [28, 31] to evaluate the RHS of the above equation.

3. Numerical results. In this section, we demonstrate the performance of the proposed SLDG and EL RK DG schemes for 2D transport equations, in terms of mass conservation, discrete GCL, high order accuracy in both space and time, numerical stability for large time-stepping size, and ability to capture discontinuities. In order to better show the advantages of the proposed schemes, we compare the results of the schemes with those of the classic RKDG method under the same settings. As in [35], the CFL number is defined by

$$CFL = \frac{\max_j \max_{\text{face}} |\mathbf{V} \cdot \mathbf{n}|}{\min_j R_j} \Delta t, \tag{3.1}$$

where R_j is the radius of the inscribed circle of the element K_j and $\mathbf{n}$ is the unit normal vector of the face of K_j;

$$R_j = 2\frac{|K_j|}{|\partial K_j|}, \tag{3.2}$$

where $|K_j|$ and $|\partial K_j|$ are the area and perimeter of K_j, respectively. By tests, we found there is little difference between the scheme with GCL correction and that without GCL correction besides the preservation capability. Thus unless otherwise noted, the EL RK DG scheme for simulations is without GCL correction.

- *Mass conservation and discrete GCL.* For all simulations, we find that the mass is conserved up to machine precision for each time step of the presented schemes, and we omit the results for brevity. The discrete GCL of EL RK DG is verified in Example 3.2.
- *Consistency.* We test the spatial and temporal accuracy by the linear transport problem, rotation, and swirling deformation flow. For the linear transport problem, we test the schemes for the problem with either periodic boundary conditions or inflow boundary conditions; the results are almost the same, and so we only present the latter in Example 3.1. For EL RK DG, the expected high order accuracy can be observed for all these tests; for the proposed P^2 SLDG, we observe the second order of convergence for solving the swirling deformation flow.
- *Stability.* The SLDG is numerically unconditionally stable and EL RK DG is numerically stable around time-stepping size of $\Delta t \sim \sqrt{h}$ in Figures 6–8. The results are consistent with those in [10].

Accepted Manuscript
Version of record at: https://doi.org/10.1137/21M1456753

- *Resolution for discontinuities.* A simple WENO limiter in [59] used for all schemes is used to control oscillations for problems with discontinuities. Note that some advanced limiters such as [58] can be applied in the proposed schemes as well. We find the SLDG and EL RK DG methods can do a better job on the resolution of solutions around discontinuities compared to RKDG.

Example 3.1 (2D linear equation). To verify the spatial accuracy of the EL RK DG method with large time-stepping size, we apply the scheme to solve the following linear equation in two dimensions up to $T = 1$:

$$u_t + u_x + u_y = 0, \quad (x, y) \in [-\pi, \pi]^2, \tag{3.3}$$

with the initial condition $u(x, y, 0) = \sin(x + y)$ and the inflow boundary conditions $u(x = -\pi, y, t) = \sin(y - \pi - 2t)$ and $u(x, y = -\pi, t) = \sin(x - \pi - 2t)$. As shown in Figure 4, the structured uniform mesh and the unstructured mesh generated by the Gmsh [27] are used to test the mesh adaptability in this example.

We report the L^1 errors and corresponding order of convergence of the P^k ($k = 1, 2$) EL RK DG scheme with $CFL = 10.2$ in Table 2. The expected $(k+1)$th orders of convergence are observed for the P^k EL RK DG scheme with either the structured uniform mesh or the unstructured mesh.

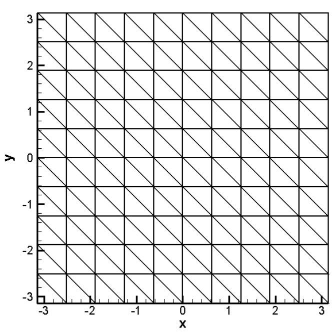

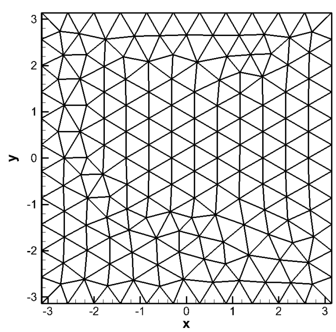

FIG. 4. *Left: The structured triangular mesh, $N = 2 \times 10^2$. Right: The unstructured triangular mesh, $N = 300$.*

TABLE 2
L^1 errors of EL RK DG schemes for linear problem, $u_t + u_x + u_y = 0, (x, y) \in [-\pi, \pi]^2$ with the initial condition $u(x, y, 0) = \sin(x + y)$ and the inflow boundary condition. $T = 1$. $CFL = 10.2$.

Structured triangular meshes					Unstructured triangular meshes				
	P^1 EL RK DG		P^2 EL RK DG			P^1 EL RK DG		P^2 EL RK DG	
Mesh	L^1 error	Order	L^1 error	Order	Mesh	L^1 error	Order	L^1 error	Order
2×20^2	1.73E-03	–	7.67E-05	–	1018	2.31E-03	–	6.98E-05	–
2×40^2	4.77E-04	1.85	8.51E-06	3.17	4132	5.47E-04	2.06	8.33E-06	3.04
2×80^2	1.09E-04	2.12	1.02E-06	3.07	16364	1.43E-04	1.95	9.24E-07	3.19
2×160^2	2.72E-05	2.01	1.01E-07	3.33	65278	3.75E-05	1.94	1.54E-07	2.59

Example 3.2 (the GCL property). To verify the GCL property of the EL RK DG method, we test the previous example with the conditions $u(x, y, 0) = 1$, $u(x =$

Accepted Manuscript
Version of record at: https://doi.org/10.1137/21M1456753

$-\pi, y, t) = 1$, $u(x, y = -\pi, t) = 1$. In the result of Proposition 2.7, the GCL property of the EL RK DG scheme relies on the time integration; we test the P^1 EL RK DG scheme with SSP-RK2 and SSP-RK3, using $CFL = 10.2$, in which the velocity field is perturbed by a random number multiplying h. The results of the EL RK DG scheme both with discrete GCL and without discrete GCL are listed in Table 3. We observe that the EL RK DG scheme without discrete GCL approximates the constant solutions in the high order accuracy; yet the EL RK DG scheme with discrete GCL exactly preserves the GCL property.

TABLE 3

GCL tests on the linear problem, $u_t + u_x + u_y = 0, (x, y) \in [-\pi, \pi]^2$, with the initial condition $u(x, y, 0) = 1$, $u(x = -\pi, y, t) = 1$, $u(x, y = -\pi, t) = 1$ at $T = 1$. P^1 EL RK DG scheme with different temporal methods, using $CFL = 10.2$, in which the velocity field is perturbed randomly. The EL RK DG scheme with discrete GCL (GCL) and without discrete GCL (no GCL).

	no GCL				GCL			
	SSP-RK2		SSP-RK3		SSP-RK2		SSP-RK3	
Mesh	L^2 error	Order	L^2 error	Order	L^2 error	Order	L^2 error	Order
1018	1.95E-05	–	7.64E-07	–	1.11E-13	–	1.11E-13	–
4132	1.17E-06	4.01	1.45E-08	5.66	2.19E-13	–	2.18E-13	–
16364	2.72E-07	2.12	2.42E-09	2.60	3.61E-13	–	3.61E-13	–
65278	2.23E-08	3.61	7.18E-11	5.09	7.75E-13	–	7.73E-13	–

Example 3.3 (rigid body rotation on a circle domain). Consider

$$u_t - (yu)_x + (xu)_y = 0, \quad (x, y) \in \{(x, y)|x^2 + y^2 \leq \pi^2\}, \tag{3.4}$$

with the initial condition $u(x, y, 0) = \exp(-3x^2 - 3y^2)$. The coarsest mesh $N = 160$ is shown in Figure 5.

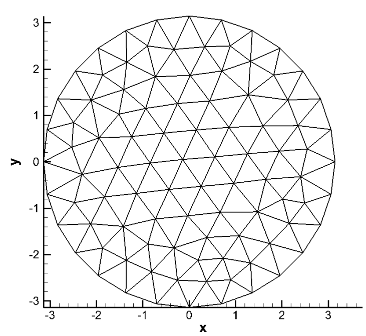

FIG. 5. *The unstructured mesh with the mesh of* 160 *is generated by GMSH.*

First, we test the spatial convergence of the proposed SLDG schemes, proposed EL RK DG schemes, and the RKDG schemes. We use the same time-stepping sizes for comparison; the CFL numbers in time step selection are set to be 0.3 for P^1 DG and 0.15 for P^2 DG. These time-stepping sizes are with the stability constraint of $1/(2k + 1)$ for RKDG. We summarize the results of these schemes for solving the problem up to $T = 2\pi$ in Table 4. We observe the expected orders of convergence and the similar results for different DG schemes.

Accepted Manuscript
Version of record at: https://doi.org/10.1137/21M1456753

Second, we study numerical stabilities of EL RK DG and SLDG schemes. We present the plots of L^1 error versus CFL of these schemes in Figure 6. We make a few observations: (1) When CFL is relatively large but smaller than the stability constraint of EL RK DG, the temporal errors starting to kick in second and third order temporal convergence order are shown. (2) Maximum CFLs with numerical stability of P^2 EL RK DG using meshes $N = 1884, 7432, 28996$ are 13.8, 19.6, 27.5, respectively. The increasing rate is around $\sqrt{2}$. (3) SLDG schemes are stable for arbitrarily large time-stepping sizes.

Third, we numerically solve the rigid body rotation (3.4) with an initial condition plotted in Figure 7(a), which consists of a slotted disk, a cone, and a smooth hump, similar to the one used in [33] for comparison purposes. In Figure 7, we present plots of the solutions solved by the P^2 RKDG, SLDG, and EL RK DG schemes with WENO limiter after one full rotation. We use CFL $= 10.2$ for SLDG and EL RK DG. We observe that (1) the solutions of SLDG and EL RK DG are comparable; (2) the solutions of SLDG and EL RK DG are less dissipative than that of RKDG, due to the fewer error accumulations of the schemes with large time-stepping size.

TABLE 4
Errors of different DG schemes for rigid body rotation on a circle domain with the initial condition $u(x, y, 0) = \exp(-3x^2 - 3y^2)$. $T = 2\pi$. The $CFL = 0.3$ for P^1 DG and $CFL = 0.15$ for P^2 DG.

Mesh	L^1 error	Order	L^1 error	Order	L^1 error	Order
	P^1 EL RK DG		P^1 SLDG		P^1 RKDG	
522	2.37E-03	–	2.37E-03	–	2.40E-03	–
1884	5.24E-04	2.35	5.24E-04	2.35	5.33E-04	2.35
7432	1.15E-04	2.21	1.15E-04	2.21	1.17E-04	2.21
28996	2.77E-05	2.09	2.77E-05	2.09	2.81E-05	2.10
	P^2 EL RK DG		P^2 SLDG		P^2 RKDG	
522	1.88E-04	–	1.89E-04	–	1.94E-04	–
1884	2.41E-05	3.20	2.41E-05	3.21	2.43E-05	3.24
7432	2.91E-06	3.08	2.91E-06	3.08	2.94E-06	3.08
28996	3.62E-07	3.07	3.62E-07	3.07	3.65E-07	3.07

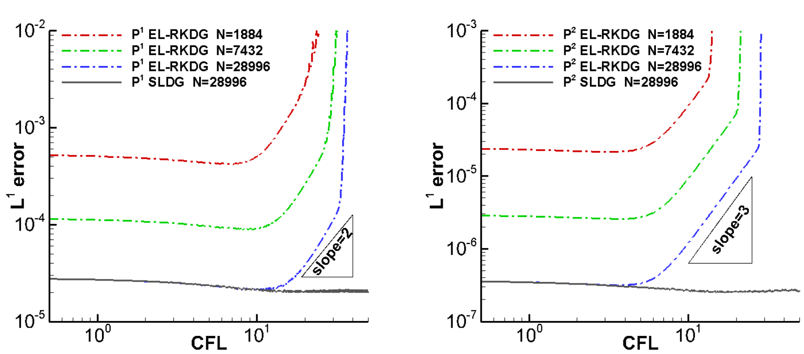

FIG. 6. *The L^1 error versus CFL of SLDG schemes and EL RK DG schemes for the rigid body rotation with $u(x, y, 0) = \exp(-3x^2 - 3y^2)$. $T = 2\pi$.*

Accepted Manuscript
Version of record at: https://doi.org/10.1137/21M1456753

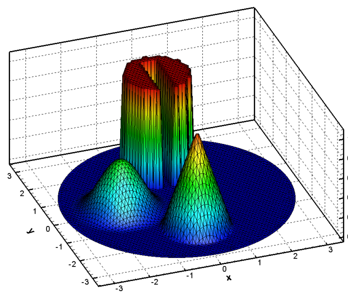

(a) initial state, $N = 7432$

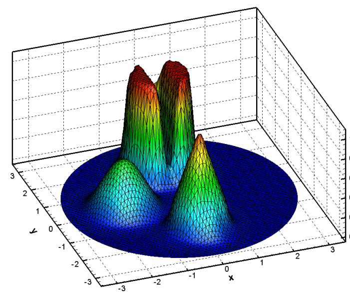

(b) P^2 RKDG, $CFL = 0.15$

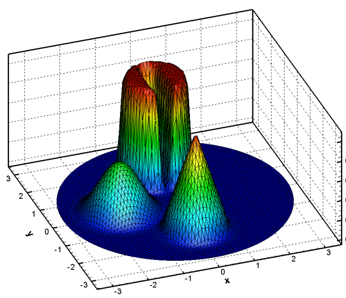

(c) P^2 SLDG, $CFL = 10.2$

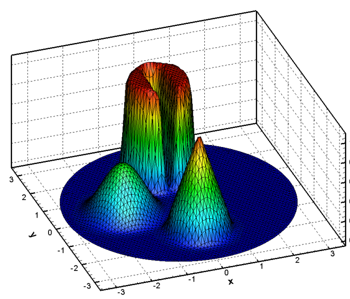

(d) P^2 EL RK DG, $CFL = 10.2$

FIG. 7. *Plots of the numerical solutions of P^2 SLDG and EL RK DG schemes for the rigid body rotation with the initial condition in* (a). $T = 2\pi$.

Example 3.4 (swirling deformation flow). We consider solving

$$u_t - \left(\cos^2\left(\frac{x}{2}\right)\sin(y)g(t)u\right)_x + \left(\sin(x)\cos^2\left(\frac{y}{2}\right)g(t)u\right)_y = 0,\ (x, y) \in [-\pi, \pi]^2, \tag{3.5}$$

where $g(t) = \cos\left(\frac{\pi t}{T}\right)\pi$ and $T = 1.5$. The initial condition is set to be the following smooth cosine bell (with C^5 smoothness):

$$u(x, y, 0) = \begin{cases} r_0^b \cos^6\left(\frac{r^b}{2r_0^b}\pi\right) & \text{if } r^b < r_0^b, \\ 0 & \text{otherwise}, \end{cases} \tag{3.6}$$

where $r_0^b = 0.3\pi$, and $r^b = \sqrt{(x - x_0^b)^2 + (y - y_0^b)^2}$ denotes the distance between (x, y) and the center of the cosine bell $(x_0^b, y_0^b) = (0.3\pi, 0)$. As in Example 3.3, we study the spatial error and the numerical stability of the proposed SLDG and EL RK DG schemes in Table 5 and Figure 8, respectively. Observations similar to those in Example 3.3 can be made for the P^1 part. We find that P^2 SLDG is of second order due to the second approximation to the sides of upstream cells, while P^2 EL RK DG is of third order. Figure 9 presents spatial errors and CPU times of the EL RK DG method and the SLDG method; we observe that with the same setting, SLDG is more expensive in CPU time to achieve the same error, compared to EL RK DG.

Accepted Manuscript
Version of record at: https://doi.org/10.1137/21M1456753

As in Example 3.3, we numerically solve the swirling deformation flow (3.5) with an initial condition plotted in Figure 10(a). The results are presented in Figure 10. Observations similar to those in Example 3.3 can be made.

TABLE 5
Errors of different DG schemes for swirling deformation flow with the smooth cosine bell. $T = 1.5$. $CFL = 0.3$ *and* 0.15 *for* P^1 *and* P^2*, respectively.*

Mesh	L^1 error	Order	L^1 error	Order	L^1 error	Order
	P^1 EL RK DG		P^1 SLDG		P^1 RKDG	
2×20^2	2.97E-03	–	2.91E-03	–	3.07E-03	–
2×40^2	7.18E-04	2.05	7.05E-04	2.05	7.64E-04	2.01
2×80^2	1.28E-04	2.49	1.26E-04	2.49	1.37E-04	2.48
2×160^2	2.25E-05	2.50	2.22E-05	2.50	2.39E-05	2.50
	P^2 EL RK DG		P^2 SLDG		P^2 RKDG	
2×20^2	4.90E-04	–	4.77E-04	–	5.10E-04	–
2×40^2	3.88E-05	3.66	4.27E-05	3.48	4.03E-05	3.66
2×80^2	3.41E-06	3.51	5.99E-06	2.83	3.51E-06	3.52
2×160^2	3.77E-07	3.18	1.26E-06	2.25	3.90E-07	3.17

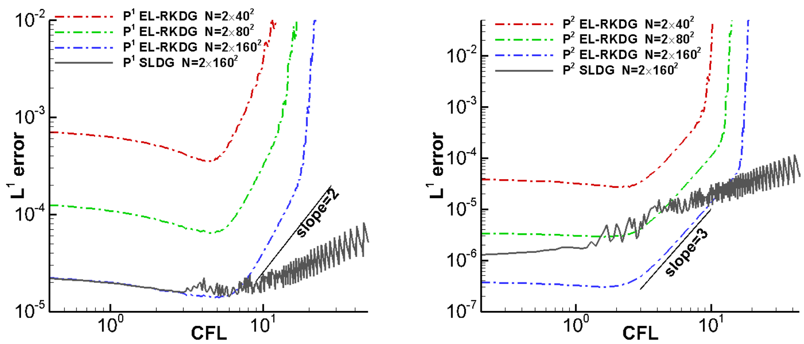

FIG. 8. *The* L^1 *error versus CFL of SLDG schemes and EL RK DG schemes for the swirling deformation flow with the smooth cosine bell.* $T = 1.5$.

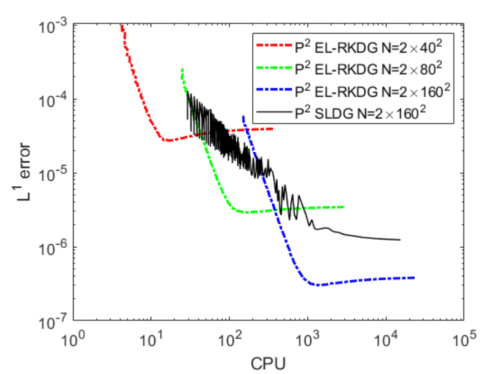

FIG. 9. *The* L^1 *error versus CPU time of SLDG schemes and EL RK DG schemes for the swirling deformation flow with the smooth cosine bell.* $T = 1.5$.

Accepted Manuscript
Version of record at: https://doi.org/10.1137/21M1456753

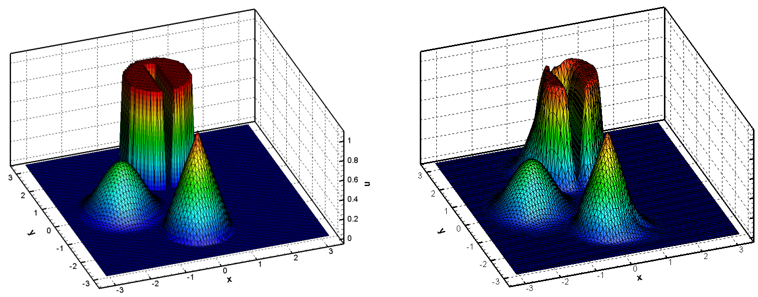

(a) initial state, $N = 2 \times 80^2$ (b) P^2 RKDG, $CFL = 0.15$

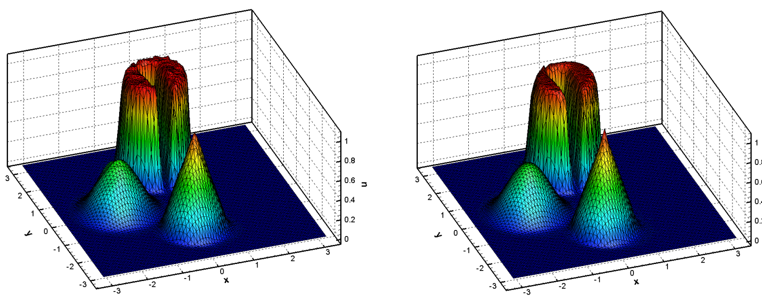

(c) P^2 SLDG, $CFL = 10.2$ (d) P^2 EL RK DG, $CFL = 10.2$

FIG. 10. *Plots of the numerical solutions of P^2 SLDG and EL RK DG schemes for the swirling deformation flow with the initial condition in (a). $T = 1.5$. $N = 2 \times 80^2$.*

4. Conclusion. We have devised the SLDG method and the EL RK DG method on the unstructured triangular meshes for linear transport problems. The crucial ingredient of the present schemes is the conservative remapping algorithm. Then the proposed schemes can be mass conservative. To the best of our knowledge, the present SLDG scheme is the first SL scheme on the unstructured mesh that can enjoy favorable properties of mass conservation, second order accuracy, and unconditionally numerical stability; the presented EL RK DG can inherit the main favorable properties and can largely alleviate the CFL constraint from RKDG. The theoretical analysis of the stability of the present schemes is a subject of our future investigation.

This is an initial effort to propose accurate and conservative semi-Lagrangian schemes for practical problems with complex geometry. Although the presented schemes are just for linear transport problems, we believe they can be extended to nonlinear transport problems via exponential integrators in [7], which has successfully coupled with the SLDG method on the structured meshes. And we believe it can also be extended for convection-diffusion equations, as in [19]. These extensions will be investigated in our future research work. As we mentioned, the semi-Lagrangian schemes are popular in climate modeling and kinetic models. Hence, it would be interesting to use this solver for these applications.

REFERENCES

[1] F. Alauzet, *A parallel matrix-free conservative solution interpolation on unstructured tetrahedral meshes*, Comput. Methods Appl. Mech. Engrg., 299 (2016), pp. 116–142.
[2] F. Alauzet and M. Mehrenberger, *P1-conservative solution interpolation on unstructured triangular meshes*, Internat. J. Numer. Methods Engrg., 84 (2010), pp. 1552–1588.
[3] N. Besse, J. Segré, and E. Sonnendrücker, *Semi-Lagrangian schemes for the two-dimensional Vlasov-Poisson system on unstructured meshes*, Transport Theory Statist. Phys., 34 (2005), pp. 311–332.
[4] N. Besse and E. Sonnendrücker, *Semi-Lagrangian schemes for the Vlasov equation on an unstructured mesh of phase space*, J. Comput. Phys., 191 (2003), pp. 341–376.
[5] O. Bokanowski and G. Simarmata, *Semi-Lagrangian discontinuous Galerkin schemes for some first-and second-order partial differential equations*, ESAIM Math. Model. Numer. Anal., 50 (2016), pp. 1699–1730.
[6] P. A. Bosler, A. M. Bradley, and M. A. Taylor, *Conservative multimoment transport along characteristics for discontinuous Galerkin methods*, SIAM J. Sci. Comput., 41 (2019), pp. B870–B902, https://doi.org/10.1137/18M1165943.
[7] X. Cai, S. Boscarino, and J.-M. Qiu, *High order semi-Lagrangian discontinuous Galerkin method coupled with Runge-Kutta exponential integrators for nonlinear Vlasov dynamics*, J. Comput. Phys., 427 (2021), 110036.
[8] X. Cai, W. Guo, and J.-M. Qiu, *A high order conservative semi-Lagrangian discontinuous Galerkin method for two-dimensional transport simulations*, J. Sci. Comput., 73 (2017), pp. 514–542.
[9] X. Cai, W. Guo, and J.-M. Qiu, *A high order semi-Lagrangian discontinuous Galerkin method for Vlasov-Poisson simulations without operator splitting*, J. Comput. Phys., 354 (2018), pp. 529–551.
[10] X. Cai, J.-M. Qiu, and Y. Yang, *An Eulerian-Lagrangian discontinuous Galerkin method for transport problems and its application to nonlinear dynamics*, J. Comput. Phys., 439 (2021), 110392.
[11] M. A. Celia, T. F. Russell, I. Herrera, and R. E. Ewing, *An Eulerian-Lagrangian localized adjoint method for the advection-diffusion equation*, Adv. Water Res., 13 (1990), pp. 187–206.
[12] N. Chalmers and L. Krivodonova, *A robust CFL condition for the discontinuous Galerkin method on triangular meshes*, J. Comput. Phys., 403 (2020), 109095.
[13] J. Cheng and C.-W. Shu, *A high order accurate conservative remapping method on staggered meshes*, Appl. Numer. Math., 58 (2008), pp. 1042–1060.
[14] Y. Cheng, I. M. Gamba, F. Li, and P. J. Morrison, *Discontinuous Galerkin methods for the Vlasov–Maxwell equations*, SIAM J. Numer. Anal., 52 (2014), pp. 1017–1049, https://doi.org/10.1137/130915091.
[15] P. G. Ciarlet, *Mathematical Elasticity, Volume* I: *Three-Dimensional Elasticity*, North-Holland, 1988.
[16] B. Cockburn and C.-W. Shu, *Runge–Kutta discontinuous Galerkin methods for convection-dominated problems*, J. Sci. Comput., 16 (2001), pp. 173–261.
[17] N. Crouseilles, P. Glanc, S. A. Hirstoaga, E. Madaule, M. Mehrenberger, and J. Pétri, *A new fully two-dimensional conservative semi-Lagrangian method: Applications on polar grids, from diocotron instability to ITG turbulence*, European Phys. J. D, 68 (2014), pp. 1–10.
[18] N. Crouseilles, M. Mehrenberger, and F. Vecil, *Discontinuous Galerkin semi-Lagrangian method for Vlasov-Poisson*, in CEMRACS'10 Research Achievements: Numerical Modeling of Fusion, ESAIM Proc. 32, EDP Sci., Les Ulis, France, 2011, pp. 211–230.
[19] M. Ding, X. Cai, W. Guo, and J.-M. Qiu, *A semi-Lagrangian discontinuous Galerkin (DG)—local DG method for solving convection-diffusion equations*, J. Comput. Phys., 409 (2020), 109295.
[20] J. Douglas, Jr. and T. R. Russell, *Numerical methods for convection-dominated diffusion problems based on combining the method of characteristics with finite element or finite difference procedures*, SIAM J. Numer. Anal., 19 (1982), pp. 871–885, https://doi.org/10.1137/0719063.
[21] D. Dunavant, *High degree efficient symmetrical Gaussian quadrature rules for the triangle*, Internat. J. Numer. Methods Engrg., 21 (1985), pp. 1129–1148.
[22] P. Farrell and J. Maddison, *Conservative interpolation between volume meshes by local Galerkin projection*, Comput. Methods Appl. Mech. Engrg., 200 (2011), pp. 89–100.
[23] P. E. Farrell, M. D. Piggott, C. C. Pain, G. J. Gorman, and C. R. Wilson, *Conservative*

interpolation between unstructured meshes via supermesh construction, Comput. Methods Appl. Mech. Engrg., 198 (2009), pp. 2632–2642.
[24] F. Filbet, E. Sonnendrücker, and P. Bertrand, *Conservative numerical schemes for the Vlasov equation*, J. Comput. Phys., 172 (2001), pp. 166–187.
[25] L. Formaggia and F. Nobile, *Stability analysis of second-order time accurate schemes for ALE–FEM*, Comput. Methods Appl. Mech. Engrg., 193 (2004), pp. 4097–4116.
[26] P. Fu, G. Schnücke, and Y. Xia, *Arbitrary Lagrangian-Eulerian discontinuous Galerkin method for conservation laws on moving simplex meshes*, Math. Comp., 88 (2019), pp. 2221–2255.
[27] C. Geuzaine and J.-F. Remacle, *Gmsh: A 3-D finite element mesh generator with built-in pre- and post-processing facilities*, Internat. J. Numer. Methods Engrg., 79 (2009), pp. 1309–1331.
[28] W. Guo, R. Nair, and J.-M. Qiu, *A conservative semi-Lagrangian discontinuous Galerkin scheme on the cubed-sphere*, Monthly Weather Rev., 142 (2013), pp. 457–475.
[29] C.-S. Huang, T. Arbogast, and C.-H. Hung, *A semi-Lagrangian finite difference WENO scheme for scalar nonlinear conservation laws*, J. Comput. Phys., 322 (2016), pp. 559–585.
[30] P. Lauritzen, R. Nair, and P. Ullrich, *A conservative semi-Lagrangian multi-tracer transport scheme (CSLAM) on the cubed-sphere grid*, J. Comput. Phys., 229 (2010), pp. 1401–1424.
[31] D. Lee, R. Lowrie, M. Petersen, T. Ringler, and M. Hecht, *A high order characteristic discontinuous Galerkin scheme for advection on unstructured meshes*, J. Comput. Phys., 324 (2016), pp. 289–302.
[32] T. Lee and C. Lin, *A characteristic Galerkin method for discrete Boltzmann equation*, J. Comput. Phys., 171 (2001), pp. 336–356.
[33] R. J. LeVeque, *High-resolution conservative algorithms for advection in incompressible flow*, SIAM J. Numer. Anal., 33 (1996), pp. 627–665, https://doi.org/10.1137/0733033.
[34] H. Liu, X. Cai, G. Lapenta, and Y. Cao, *Conservative semi-Lagrangian kinetic scheme coupled with implicit finite element field solver for multidimensional Vlasov Maxwell system*, Commun. Nonlinear Sci. Numer. Simul., 102 (2021), 105941.
[35] D. Luo, W. Huang, and J. Qiu, *A quasi-Lagrangian moving mesh discontinuous Galerkin method for hyperbolic conservation laws*, J. Comput. Phys., 396 (2019), pp. 544–578.
[36] K. Morton, A. Priestley, and E. Suli, *Stability of the Lagrange-Galerkin method with non-exact integration*, ESAIM Math. Model. Numer. Anal., 22 (1988), pp. 625–653.
[37] K. W. Morton, *On the analysis of finite volume methods for evolutionary problems*, SIAM J. Numer. Anal., 35 (1998), pp. 2195–2222, https://doi.org/10.1137/S0036142997316967.
[38] P.-O. Persson, J. Bonet, and J. Peraire, *Discontinuous Galerkin solution of the Navier–Stokes equations on deformable domains*, Comput. Methods Appl. Mech. Engrg., 198 (2009), pp. 1585–1595.
[39] O. Pironneau, *On the transport-diffusion algorithm and its applications to the Navier-Stokes equations*, Numer. Math., 38 (1982), pp. 309–332.
[40] J.-M. Qiu and C.-W. Shu, *Conservative high order semi-Lagrangian finite difference WENO methods for advection in incompressible flow*, J. Comput. Phys., 230 (2011), pp. 863–889.
[41] M. Restelli, L. Bonaventura, and R. Sacco, *A semi-Lagrangian discontinuous Galerkin method for scalar advection by incompressible flows*, J. Comput. Phys., 216 (2006), pp. 195–215.
[42] B. Riviere, *Discontinuous Galerkin Methods for Solving Elliptic and Parabolic Equations: Theory and Implementation*, Frontiers Appl. Math. 35, SIAM, Philadelphia, 2008, https://doi.org/10.1137/1.9780898717440.
[43] J. A. Rossmanith and D. C. Seal, *A positivity-preserving high-order semi-Lagrangian discontinuous Galerkin scheme for the Vlasov–Poisson equations*, J. Comput. Phys., 230 (2011), pp. 6203–6232.
[44] T. Russell and M. Celia, *An overview of research on Eulerian-Lagrangian localized adjoint methods (ELLAM)*, Adv. Water Res., 25 (2002), pp. 1215–1231.
[45] C.-W. Shu and S. Osher, *Efficient implementation of essentially non-oscillatory shock-capturing schemes*, J. Comput. Phys., 77 (1988), pp. 439–471.
[46] Z. Si, J. Wang, and W. Sun, *Unconditional stability and error estimates of modified characteristics FEMs for the Navier–Stokes equations*, Numer. Math., 134 (2016), pp. 139–161.
[47] I. E. Sutherland and G. W. Hodgman, *Reentrant polygon clipping*, Comm. ACM, 17 (1974), pp. 32–42.
[48] Z. Tao, W. Guo, and Y. Cheng, *Sparse grid discontinuous Galerkin methods for the Vlasov-Maxwell system*, J. Comput. Phys. X, 3 (2019), 100022.
[49] P. D. Thomas and C. K. Lombard, *Geometric conservation law and its application to flow*

computations on moving grids, AIAA J., 17 (1979), pp. 1030–1037.

[50] S. Tirupathi, J. S. Hesthaven, Y. Liang, and M. Parmentier, *Multilevel and local time-stepping discontinuous Galerkin methods for magma dynamics*, Comput. Geosci., 19 (2015), pp. 965–978.

[51] J. G. Trulio and K. R. Trigger, *Numerical Solution of the One-Dimensional Hydrodynamic Equations in an Arbitrary Time-Dependent Coordinate System*, University of California Lawrence Radiation Laboratory Report UCLR-6522, Lawrence Berkeley National Laboratory, Berkeley, CA, 1961.

[52] H. Wang, R. Ewing, G. Qin, S. Lyons, M. Al-Lawatia, and S. Man, *A family of Eulerian-Lagrangian localized adjoint methods for multi-dimensional advection-reaction equations*, J. Comput. Phys., 152 (1999), pp. 120–163.

[53] J. Wang, Z. Si, and W. Sun, *A new error analysis of characteristics-mixed FEMs for miscible displacement in porous media*, SIAM J. Numer. Anal., 52 (2014), pp. 3000–3020, https://doi.org/10.1137/130939717.

[54] Y. Yang, X. Cai, and J.-M. Qiu, *Optimal convergence and superconvergence of semi-Lagrangian discontinuous Galerkin methods for linear convection equations in one space dimension*, Math. Comp., 89 (2020), pp. 2113–2139.

[55] A. Younes, P. Ackerer, and F. Lehmann, *A new efficient Eulerian–Lagrangian localized adjoint method for solving the advection–dispersion equation on unstructured meshes*, Adv. Water Res., 29 (2006), pp. 1056–1074.

[56] M. Zhang, W. Huang, and J. Qiu, *High-order conservative positivity-preserving DG-interpolation for deforming meshes and application to moving mesh DG simulation of radiative transfer*, SIAM J. Sci. Comput., 42 (2020), pp. A3109–A3135, https://doi.org/10.1137/19M1297907.

[57] X. Zhang, *On positivity-preserving high order discontinuous Galerkin schemes for compressible Navier–Stokes equations*, J. Comput. Phys., 328 (2017), pp. 301–343.

[58] J. Zhu, C.-W. Shu, and J. Qiu, *High-order Runge-Kutta discontinuous Galerkin methods with a new type of multi-resolution WENO limiters on triangular meshes*, Appl. Numer. Math., 153 (2020), pp. 519–539.

[59] J. Zhu, X. Zhong, C.-W. Shu, and J. Qiu, *Runge–Kutta discontinuous Galerkin method using a new type of WENO limiters on unstructured meshes*, J. Comput. Phys., 248 (2013), pp. 200–220.